# Supplementary Material for

# AsiaRiceMap10m: high-resolution annual paddy rice maps for Southeast and Northeast Asia from 2017 to 2019

Jichong Han[1], Zhao Zhang[1], Yuchuan Luo[1], Juan Cao[1], Liangliang Zhang[1], Fei Cheng[1], Huimin Zhuang[1], Jing Zhang[1]

[1]State Key Laboratory of Earth Surface Processes and Resource Ecology/ MoE Key Laboratory of Environmental Change and Natural Hazards, Faculty of Geographical Science, Beijing Normal University, Beijing 100875, China

*Correspondence to*: Zhao Zhang (sunny_zhang@bnu.edu.cn)



**Contents**

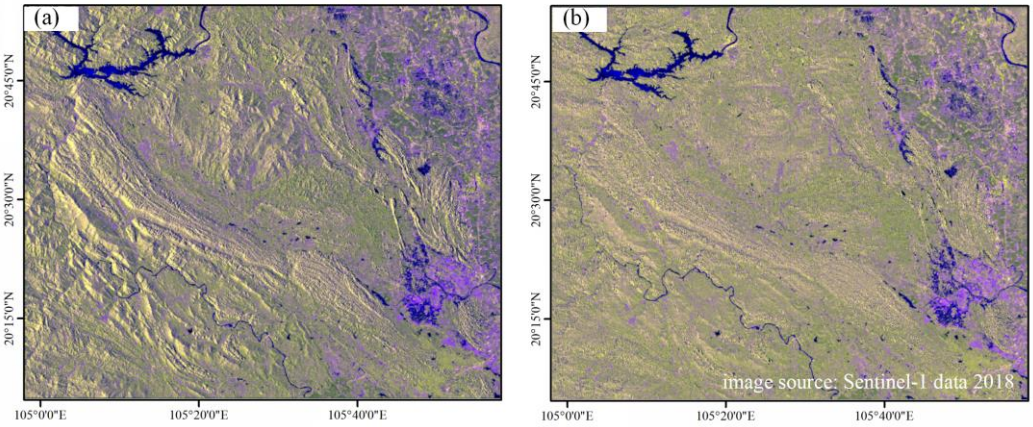


Figure S1. Sentinel-1 RGB color composite over the typical area in Vietnam in 2018 before correction (a) and after correction (b) with a physical volume model. (R/G/B: VV, VH, and VV/VH).

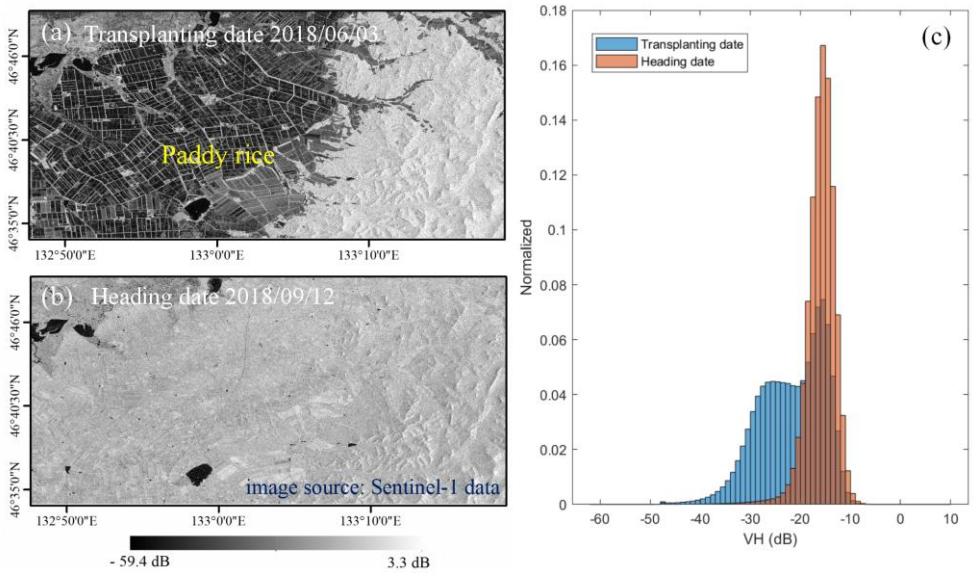


Figure S2. VH polarization backscatter images on the paddy rice transplanting date (a) and heading date (b), and normalized histogram of the images (c).

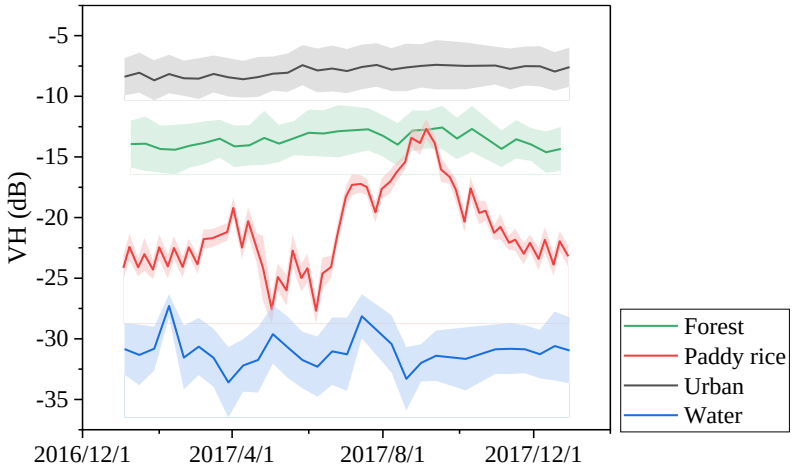


Figure S3. The seasonal dynamics of VH backscatter coefficients for different land cover types from random sample blocks with 100m radius. The profile was generated from the following random points: forest (20.232934°N, 103.552905°E), paddy rice (47.665726°N, 133.018530°E), urban (21.003088°N, 105.827390°E), water (12.974382°N, 103.940706°E). The light-shaded areas indicate the standard deviation.

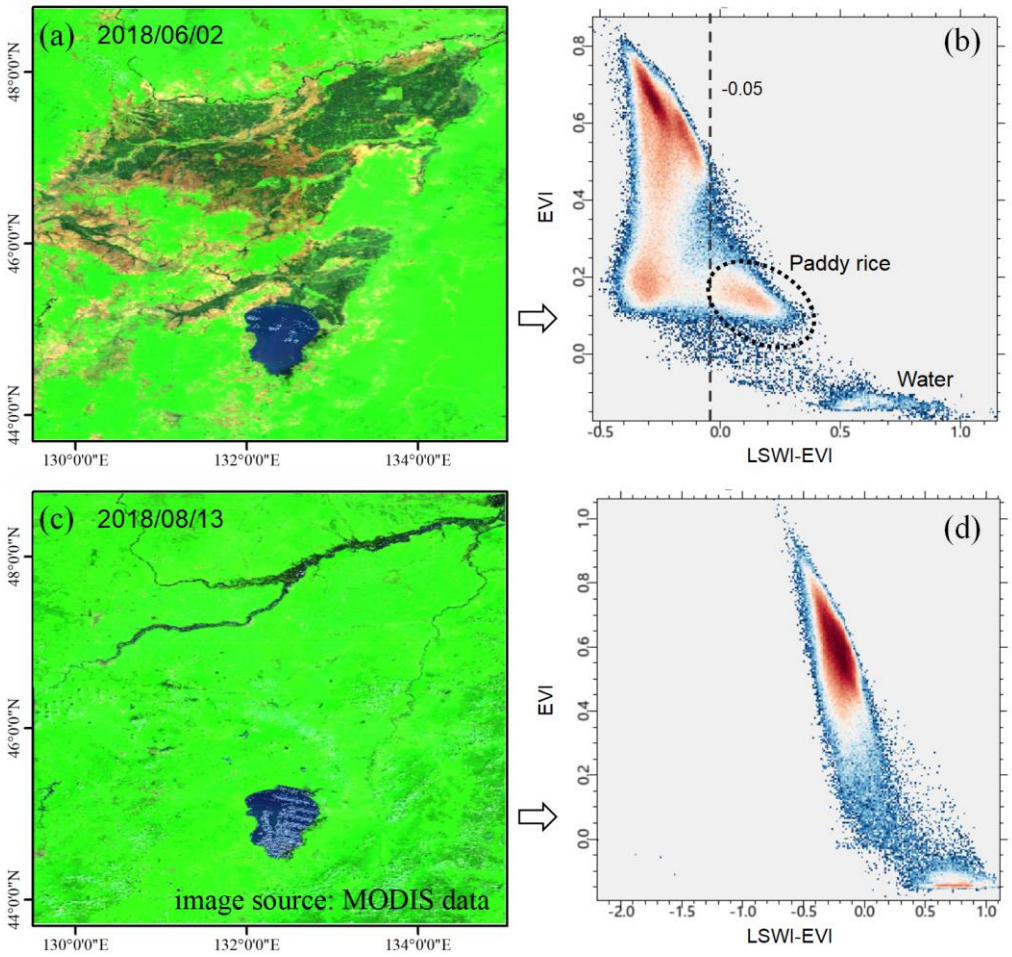


Figure S4. Spatial-temporal dynamics of flooded (a, b) and open canopy (c, d) for rice paddy fields in Northeast China. (a, c) Composite MODIS images displayed with SWIR2 band, NIR band, and blue band (R/G/B=band7/band2/band1). (b, d) the corresponding 2-D scatter plots of vegetation indices (EVI and LSWI) and the difference between them from the MODIS data. The color density represents the number of pixels.

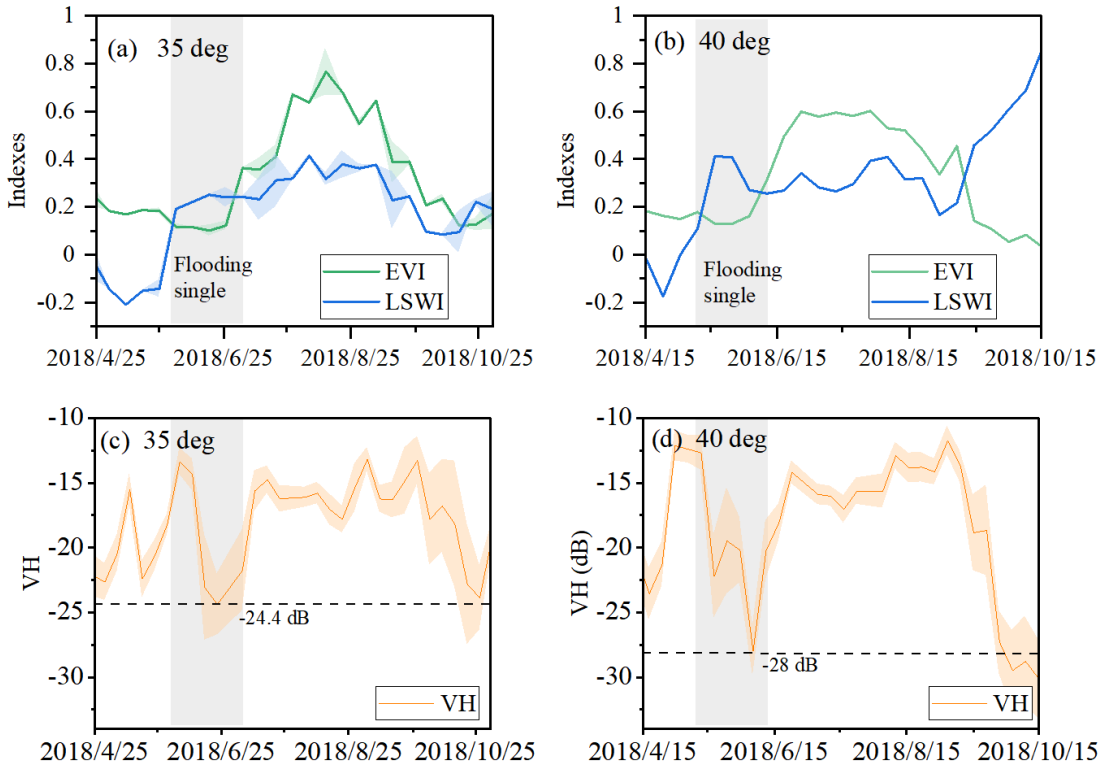


Figure S5. The seasonal dynamics of vegetation indices (EVI and LSWI) and backscattering coefficient (VH) of paddy rice at different incidence angles for Sentinel-1. (a, c) 35 deg. (b, d) 40 deg. The light-shaded areas indicate the standard deviation.

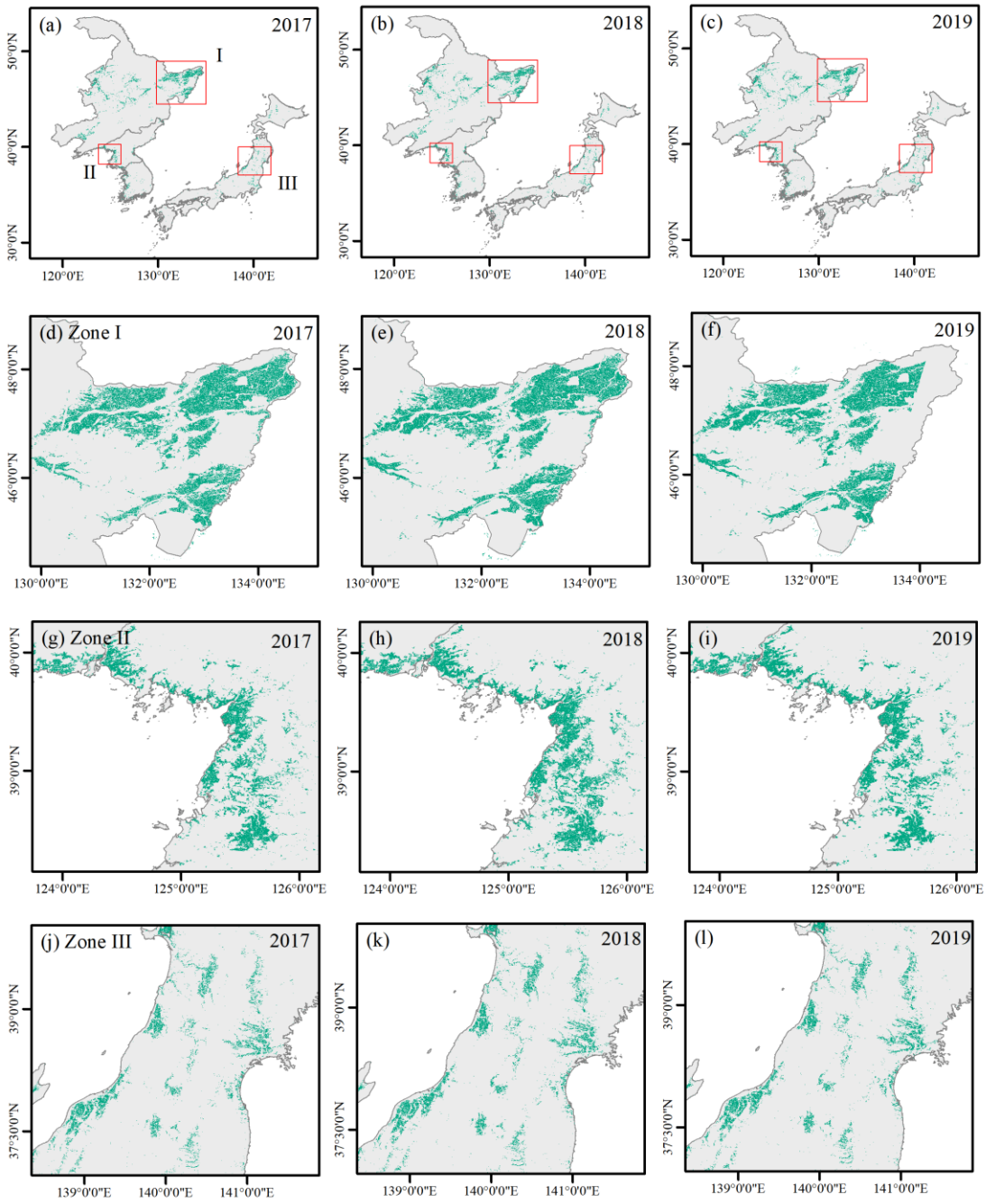


Figure S6. Spatial distribution of annual paddy rice fields with 10m resolution in Northeast Asia during 2017 - 2019 derived by our improved method (a-c). (d-l): the zoomed-in maps displaying detailed information in local zones. Find the example data for (d-l) here (https://doi.org/10.17632/cnc3tkbwcm.1 , example05-13).

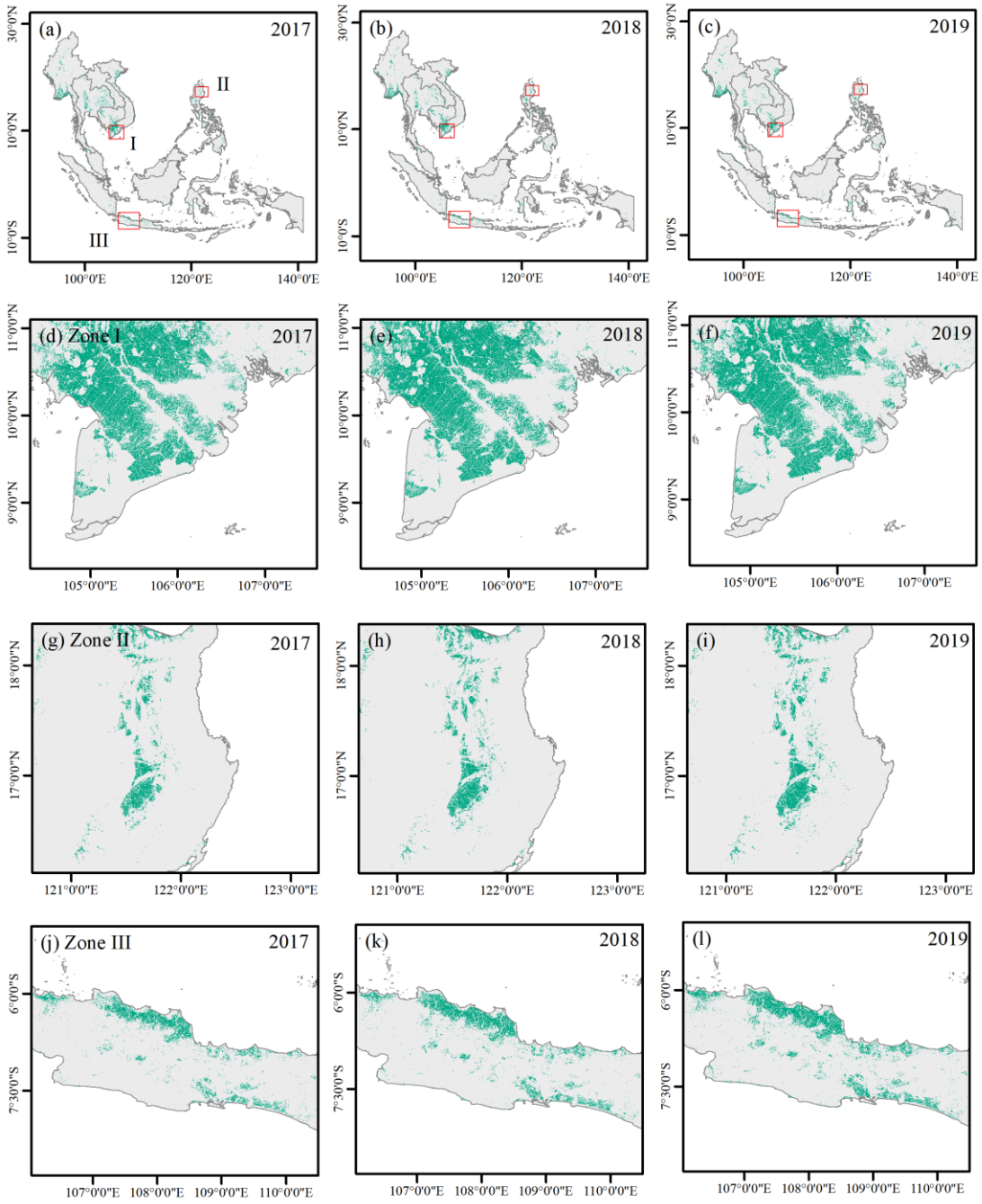


Figure S7. Spatial distribution of annual paddy rice fields with 10m resolution in Southeast Asia in 2017 - 2019 derived by our improved method (a-c). (d-l): the zoomed-in maps displaying detailed information in local zones. Find the example data for (d-l) here (https://doi.org/10.17632/cnc3tkbwcm.1 , example14-22).

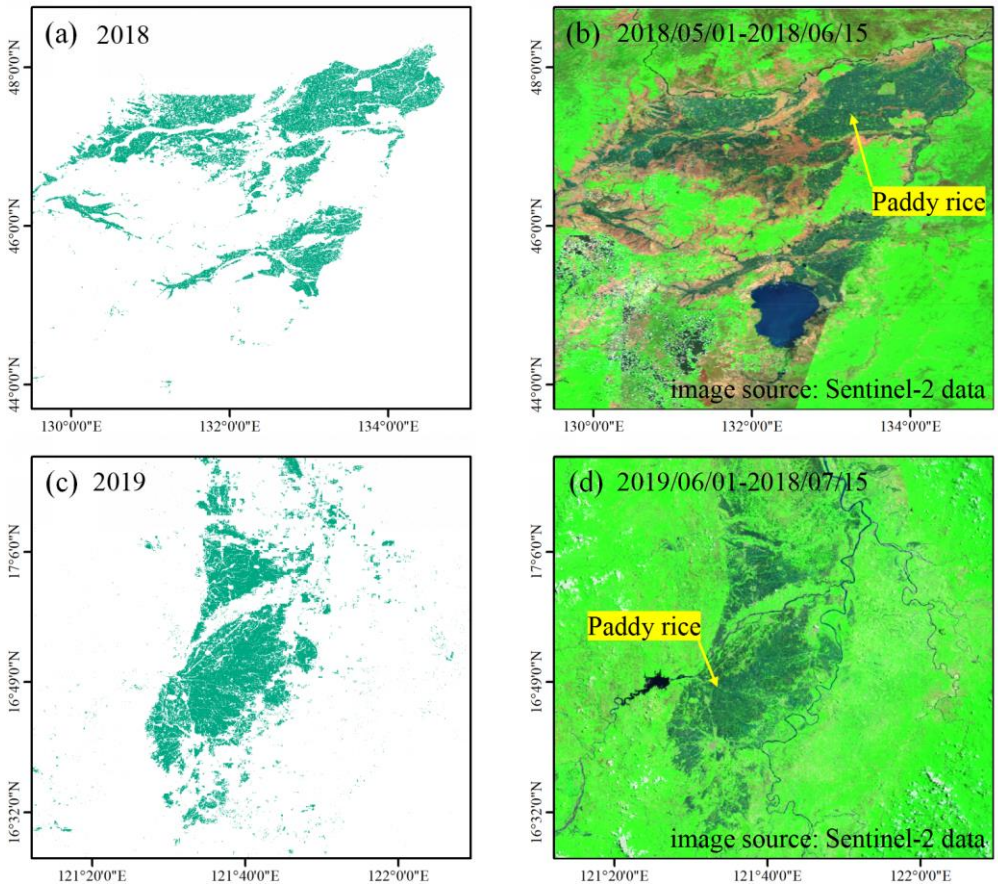


Figure S8. Comparison of classification results (a, c) with high-resolution optical images (b, d) from paddy rice transplanting period in typical areas. Sentinel-2 median images are composite displayed with SWIR2 band, NIR band, and blue band (R/G/B = band12/band8/band4).

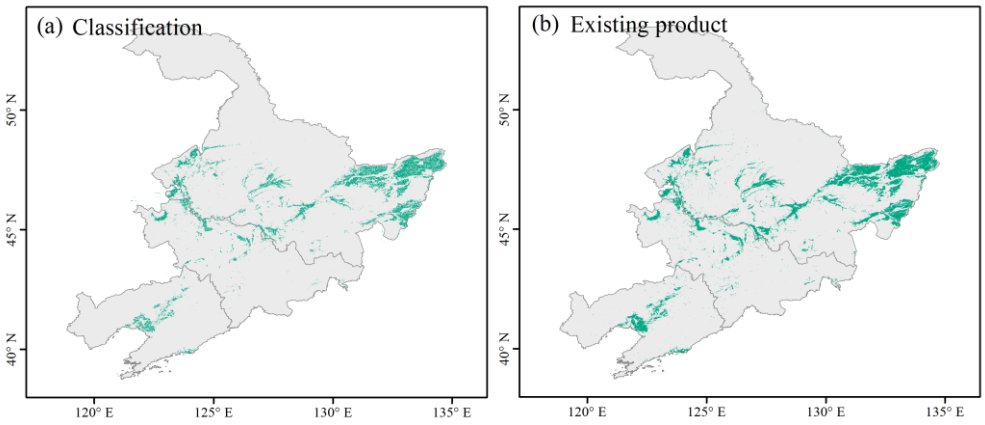


Figure S9. Comparison of our paddy rice map (a) with the existing MODIS-based map (b) in Northeast China in 2017.

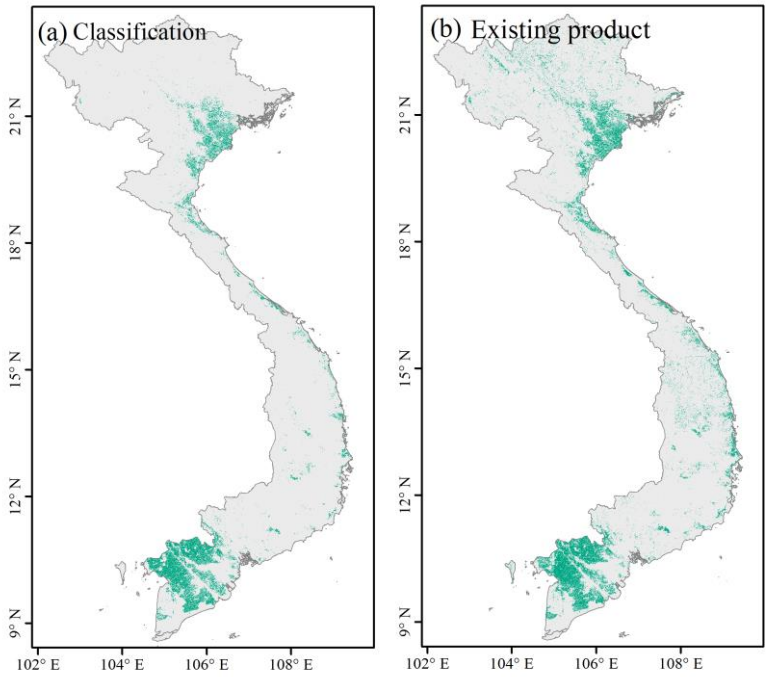


Figure S10. Comparison of our paddy rice map (a) with the existing map (b) (Paddy fields on the JAXA map) in Vietnam in 2017.

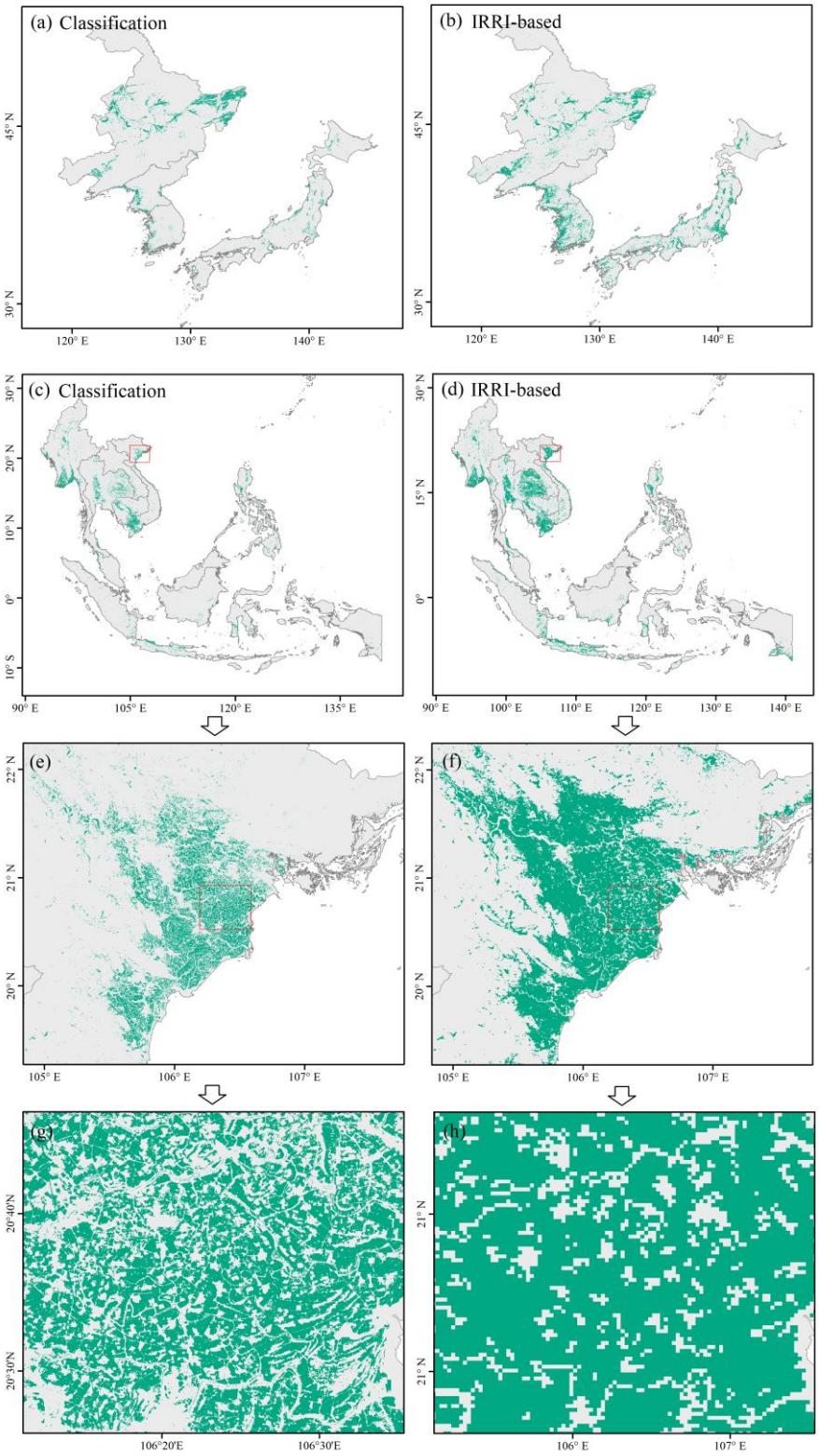


Figure S11. Paddy rice maps of Northeast and Southeast Asia. (a, c, e, and g) were derived by our method. (b, d, f, and h) are the International Rice Research Institute (IRRI)-based rice map. Note that the periods between our paddy rice maps (2017-2019) and the IRRI-based data products (2000-2012) are different. The purpose of the comparison is for a general verification of the paddy rice distribution.